ORIGINAL ARTICLE

Enabling Radioprotection Capabilities in Next Generation Wireless Communication Systems: An Ecological Green Approach

Charilaos C. Zarakovitis[1,2]* | **Qiang Ni[1]*** |
Michail-Alexandros Kourtis[2]

[1]School of Computing and Communications, Lancaster University, Bailrigg, LA1 4WA, UK (e-mail: {c.zarakovitis, q.ni}@lancaster.ac.uk)

[2]Media Networks Laboratory, Institute of Informatics and Telecommunications, National Centre for Scientific Research "Demokritos", Aghia Paraskevi, 153 41, Greece (e-mail: {akis.kourtis, c.zarakovitis}@iit.demokritos.gr)

Correspondence
Qiang Ni
Email: q.ni@lancaster.ac.uk

In future 5G and beyond radio systems, access points equipped with massive antennas will be deployed to support the increased communication demands. As a result, radio environments will become more dense and users will be exposed to higher electromagnetic field (EMF) radiation from wireless devices than today. This paper proposes to take preemptive action towards protecting the public health from potential EMF-related ill effects by examining radiation-aware solutions for future green wireless communication systems from the radio resource scheduling perspective. Our efforts focus on correlating the transmit power levels of the wireless system with the operands used to express the EMF dosimetry metrics known as maximum permissible exposure (MPE) and specific absorption rate (SAR). In addition, we formulate power minimisation problems subject to the MPE and SAR safety standards, and the individual user quality of service (QoS) demands to derive convex optimisation-based solution of dynamic subcarrier allocation and adaptive power management. The simulation results confirm that our green solution reduces significantly the user exposure to radiation, while providing the required QoS. We expect that our findings can kickoff new research directions for controlling the public exposure to radiation from wire-

less devices in dense networks towards safer 5G communication systems.

1 | INTRODUCTION

Wireless communication systems are, and will remain, an inevitable part of our lives. Yet their beneficial use may come at a price of potential adverse health and ecological effects of electromagnetic field (EMF) emission/radiation. In its latest report (June 2013) to the Public Health England, the UK Advisory Group on Non-Ionising Radiation acknowledged a substantial body of epidemiological research published on cancer risks in relation to wireless mobile phone use [1]. Also, in a recent press release (May 2016) the US National Toxicology Program announced risk assessments of human exposure to EMF emission from wireless devices with symptoms including but are not limited to mental diseases, tissue impairment, low sperm motility and brain tumor [2]. More importantly, the differences in children's anatomy make them significantly more vulnerable than adults, e.g., children absorb at least double the radiation as adults [3]. Risks go well beyond those to humans as there is a growing proof of deterioration effects to plant and animal life too [4]-[5]. The discussion and conclusions on such ill effects have triggered formidable concerns to scientists and citizens about whether wireless technology is, and will be, safe for the public health and ecosystem.

In an effort to address such concerns, the World Health Organisation (WHO) and the Australian radiation protection and nuclear safety agency (ARPANSA) advise that public health disciplines should focus on minimising the daily exposure to EMF and encourages precautionary approaches like reducing the use of cell phones, using hands-free or earpieces, and limiting the use of mobile devices by pregnant women and children among others [6]. While those precautionary approaches may help mitigate ill effects in the short-term, we believe the proposition that in order to adequately protect public and health ecosystems we must design future radio-efficient wireless communication solutions capable of reducing significantly wireless EMF emission. Potential approaches would be to investigate important features of *radiation-awareness* pertaining to the exposure metrics established by the UK National Radiological Protection Board (NRPB) with respect to the dosimetry of human exposure to EMF emission in the radiated far- and near-field, known as the maximum permissible exposure (MPE) (in W/cm2) and specific-absorption rate (SAR) (in W/Kg), respectively [7]. The main focus of MPE and SAR radiation metrics is to evaluate and manage power deposition in human tissue from fixed-position and portable devices, respectively [8]. In consequence, controlling the transmit power levels according to channel conditions of wireless devices can bring about sufficient reduction of users' exposure to radiation towards "greener" communication systems.

Open issues and motivation

Most radiation-aware approaches reported focus on reducing the MPE and SAR levels of wireless communication systems using *hardware enchantments*. A popular technique is the use of *electromagnetic bandgap* (EBG) structure [9], which acts as a perfect magnetic conductor surface to suppress surface waves and reduce undesired radiation from emitting antennas. Another prevalent method is the application of ferrite materials and metamaterials between the antenna and the user's head (mainly used in 900-1800 MHz bands) [10]-[11]. For example, [10] shows that using a ferrite sheet as protection attachment between the antenna and user's head can significantly reduce the SAR levels,

while [11] enhances radiation efficiency using a perfect electric conductor reflector placed between the head and the driver of a folded loop antenna. Moreover, [12] and [13] show that the position of the shielding material is an important factor for SAR reduction effectiveness by examining the effect of conductive materials to cellular phone radiation under various scenarios of user exposure.

Besides the available hardware-based techniques, radiation-awareness can be intelligently enhanced using radio resource scheduling frameworks to systematically allocate the wireless resources according to MPE and SAR safety thresholds. To the best of our knowledge, limited research has been committed to develop such frameworks, which have the potential to enable the radio-protection properties in more cost-effective and flexible manner than hardware-based approaches. For example, [14] shows that by bounding SAR into a two antenna beamforming-based resource scheduling strategy can bring about 3-4dB gain in equivalent transmit power than formulating the beamforming strategy without SAR considerations. Also, some recent studies on wireless power transfer (WPT) consider radio-protection properties in their optimisation analysis to report substantial capacity gains and/or power saving compared to relevant radiation unaware approaches [15]-[17]. Other recent work tries to reduce power level by maximising energy efficiency and radio resource mangement approaches [18]-[21]. However, none of the abovementioned research has considered the following issues jointly: (i) satisfying the users' quality of service (QoS) requirements, (ii) addressing dynamic subcarrier allocation policy, (iii) expressing the MPE and SAR metrics by means of power and subcarrier operands at network physical layer (commonly MPE and SAR functions are related to the incident power density), (iv) considering various levels for MPE and SAR according to user's physical characteristics (adults, children, male female), etc. These open issues motivate the proposed work in this paper.

Scope, novelty and contributions

The scope of this work is to enable radiation-awareness in next generation green wireless communication systems by bounding the optimisation of radio resource scheduling with policies for EMF radio-protection and transmit power mitigation. The novelty of this work is that it is the first attempt to consider the MPE and SAR metrics jointly into the radio resource scheduling design. Most relevant attempts neither realise the exposure of system users to radiation from wireless devices, or they consider each MPE or SAR metric individually, which imposes radically different system modeling and optimisation than considering those two key metrics jointly as we consider in this new approach. The contributions of this work are summarised below:

- We develop green radio resource scheduling framework to systematically control the trade-off between user exposure to EMF radiation and QoS requirements, which has yet been studied in earlier contributions.
- We express the MPE and SAR formulas with respect to the subcarrier indexing and power allocation operands at physical layer such that the new expressions can be smoothly applied on optimisation problems for green radios.
- We propose low-complexity solution of dynamic subcarrier and adaptive power distributions with guaranteed convergence, and evaluate its green performance using extended comparisons with related approaches.

The rest of the paper is organised as follows. Section 2 presents the system modeling and formulates the green optimisation problem. Section 3 expresses the MPE and SAR by means of subcarrier and power operands at physical layer, while Section 4 derives the optimal solution with radio-protection awareness principle. Section 5 examines key properties of the proposed solution, while Section 6 evaluates the green performance of the outcomes using simulation comparisons with relevant studies. Section 7 finally concludes this paper.
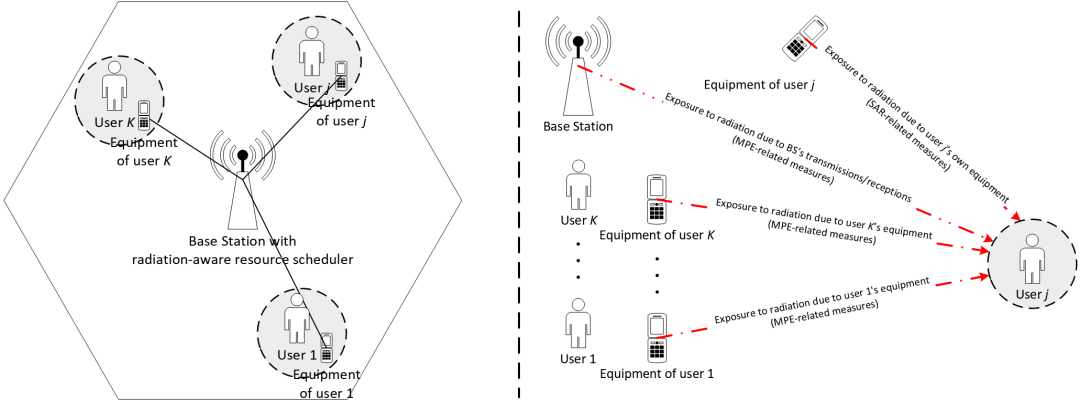
FIGURE 1 Illustration of the multi-user single-cell OFDMA system model (left) with representation of exposure of the j-th user due to radiation from transceivers at the BS and the nearby user equipments (right).

2 | SYSTEM MODELING AND PROBLEM FORMULATION FOR RADIATION-AWARE WIRELESS SYSTEMS

We focus on downlink[1] transmissions in single-cell wireless network consisted by one base station (BS) and K total mobile users. The BS is placed at the center of the cell and it performs the subcarrier and power scheduling, while the mobile users share N subcarriers of total bandwidth BW using orthogonal frequency division multiple access (OFDMA).

In this regard, each mobile user can be exposed to (i) radiation at the far-field (i.e. MPE-related measures) caused by the $N \times K$ transmissions between the BS and all mobile users, and (ii) radiation at the near-field (i.e. SAR-related measures) issued by the transmissions/receptions between the user equipment and user body, as shown in Figure 1. To enable the radiation-awareness property in such network we deploy at the BS a radio resource controller to assign the available subcarriers to different users, while allocating the minimum amount of transmit power on respective subcarriers. The green radio resource scheduling problem we consider is to optimise the subcarrier and power assignments so as to minimise the overall transmit sum-power in the network, while satisfying the required MPE, SAR and QoS constraints. Mathematically, the given problem is formulated as follows.

$$\min_{s_{ij} \in \{0,1\}, p_{ij} \geq 0} \sum_{j=1}^{K} \sum_{i=1}^{N} \left(s_{ij} \cdot p_{ij} \right) \tag{1}$$

subject to:
$$s_{ij} \in \{0, 1\}, \quad \forall ij, \tag{2}$$

$$\sum_{j=1}^{K} s_{ij} \leq 1, \quad \forall i, \tag{3}$$

$$P^{Tx} = \sum_{j=1}^{K} \sum_{i=1}^{N} \left(s_{ij} \cdot p_{ij} \right) \leq P_T, \tag{4}$$

$$p_{ij} \geq 0, \quad \forall ij, \tag{5}$$

---

[1]Similar design approach can be considered for uplink direction and/or either for frequency division duplex (FDD) or time division duplex (TDD) transmission mode.

$$r_j = \frac{BW}{N} \cdot \left(\sum_{i=1}^{N} s_{ij} \cdot \log_2 \left(1 + \left(p_{ij} \cdot \frac{|h_{ij}|^2}{\Gamma \cdot \frac{N_0 \cdot BW}{N}} \right) \right) \right) \geq q_j, \quad \forall j, \tag{6}$$

$$MPE \leq MPE^{\text{limit}}, \tag{7}$$

$$SAR_{j/1g,10g} \leq SAR_{1g,10g}^{\text{limit}}, \quad \forall j, \tag{8}$$

where s_{ij} denotes the subcarrier indexing of user $j = 1, ..., K$ and subcarrier $i = 1, ..., N$, $p_{ij} \geq 0$ the allocated power (in dBm), h_{ij} the instantaneous channel gain[2] (in dB), r_j the instantaneous data rate of user j (in bit/sec), N_0 the power spectral density of additive white Gaussian noise (in V^2/Hz) and Γ the signal-to-noise ratio (SNR) gap[3] (in dB). More precisely, the optimisation objective (1) of problem (1)-(8) represents the radiating sum-power transmitted from the BS to all K users. Subcarrier allocation constraints (2) and (3) bound the subcarrier indexing (i.e. $s_{ij} = 1$ if subcarrier i is allocated to user j and $s_{ij} = 0$, otherwise) and certify that a subcarrier can be allocated to no more than one user, respectively. Also, transmit power constraints (4) and (5) ensure transmission feasibility by limiting the total sum-power radiated from the BS to all users and subcarriers P^{Tx} by the total available power at the BS P_T, while QoS constraint (6) guarantees the satisfaction of the minimum data rate requirement q_j of each individual user j. Moreover, the radiation exposure constraints (7) and (8) indicate that system's MPE and each user's SAR levels (i.e. $SAR_{j/1g,10g}$) should not exceed the predefined WHO/NRPB radiation thresholds, denoted by MPE^{limit} and $SAR_{1g,10g}^{\text{limit}}$, respectively.

An issue arises as most relevant research have expressed the MPE and SAR quantities in equations (7) and (8) with respect to the incident power density and/or electric field strength, which are difficult to calculate and handle during the optimisation analysis. To bypass this issue, next Section III correlates MPE and SAR with the optimisation operands s_{ij} and p_{ij} at physical layer, which simplifies the optimisation analysis.

3 | MPE AND SAR ESTIMATION FORMULAS FOR RADIO RESOURCE SCHEDULING PROBLEMS

According to WHO/NRPB, the mathematical expression for *MPE* is given by [14]

$$MPE = \frac{P^{Tx} \cdot G}{4 \cdot \pi \cdot \delta^2}, \tag{9}$$

where G is the numerical gain of the BS's transmitting antenna relative to an isotropic source, (in dBm), and δ the radial distance between the BS's antenna and system users given by $\delta = \sqrt{\text{horizondial\_distance}^2 + \text{vertical\_distance}^2}$ (in meter). Therefore, using (9) and having knowledge of the antenna's dimensions, position and radiating properties, the MPE system constraint (7) can be reformulated by means of the allocation operands s_{ij} and p_{ij}, as

$$\frac{G}{4 \cdot \pi \cdot \delta^2} \cdot \underbrace{\sum_{j=1}^{K} \sum_{i=1}^{N} \left(s_{ij} \cdot p_{ij} \right)}_{P^{Tx}} \leq MPE^{\text{limit}} \Rightarrow$$

---

[2] In this work, we assume that the channel state information (CSI) is perfectly known to the BS. To produce more realistic approach, imperfect CSI can be also considered, which however is out of the scope of this work, which mainly focuses on how to introduce the radiation-awareness principle in radio resource scheduling.

[3] The Γ gap of r_{ij} in (6) can be used to capture the difference between the SNR needed to achieve a certain r_{ij} for a practical system and its theoretical data rate limit, i.e., if practical signal constellations are to be used during simulations (e.g. quadrature amplitude modulation (QAM)), Γ can straightforward signify the bit-error-rate (BER) requirement.

$$P^{Tx} \leq MPE^{\text{limit}'} \quad (\text{in W/cm}^2), \tag{10}$$

with $MPE^{\text{limit}'} = \frac{4 \cdot \pi \cdot \delta^2 \cdot MPE^{\text{limit}}}{G}$. Equation (10) bounds the user exposure to radiation from all network emitting antennas placed in $\delta > 50$mm distance from the mobile user's body. For $\delta < 50$mm the exposure of j−th user is mainly due to its own wireless equipment and it is given by [11]-[13]

$$SAR_{j/1g,10g} = \frac{\sigma_j(f) \cdot E^2}{\rho_j(f)}, \tag{11}$$

where E^2 in (11) is the total root mean square (RMS) electrical field strength (in V/meter), $\sigma_j(f)$ the frequency f dependent coefficient to represent the conductivity of the user's tissue-simulating material (in Siemens/meter), and $\rho_j(f)$ the frequency dependent coefficient to represent the mass density of user's tissue-simulating material (in Kg/m^3). Notice that although the simplicity of MPE reformulation, the quantity of $SAR_{j/1g,10g}$ is more difficult to correlate with s_{ij} and p_{ij} because E^2 in (11) cannot be calculated but only measured in practice using laboratory equipment including mannequins, electrolytes, robotically controlled probes, etc. [11]-[13]. However, *measuring E^2* at each transmission/reception cycle is not convenient as the resource scheduling process should operate in real-time [14]. Instead, theoretical formulas that can *estimate $SAR_{j/1g,10g}$* have higher practical importance such as the generalised estimation[4]

$$SAR_{j/1g,10g} = \Omega_j(f) \cdot P_j^{Tx}, \tag{12}$$

$$\begin{aligned}
\Omega_j(f) = {} & \frac{249.75 \cdot \sigma(f)}{R(f)_{wb/1g,10g} \cdot \omega \cdot \Phi_{3dB} \cdot L \cdot \delta \cdot \rho(f)} \cdot \left| \frac{2}{1+\sqrt{\varepsilon}} \right|^2 \times \\
& \sqrt{\frac{\mu}{\varepsilon_0}} \cdot \left[\frac{\mu \cdot \varepsilon_r' \cdot \varepsilon_0}{2} \cdot \left(\sqrt{1 + \left(\frac{\sigma(f)}{\omega \cdot \varepsilon_r' \cdot \varepsilon_0} \right)^2} - 1 \right) \right]^{-\frac{1}{2}} \times \\
& \left[1 + \left(\frac{4 \cdot \pi \cdot \delta}{\Phi_{3dB} \cdot G_A \cdot L} \right)^2 \right]^{-\frac{1}{2}},
\end{aligned} \tag{13}$$

with $\Omega_j(f)$ the j−th user's characteristic function with respect to emitting antenna position and side of exposure (summarised in Table 1), and P_j^{Tx} the power transmitted form BS to user j over the allocated subcarriers to this user, i.e., $P_j^{Tx} = \sum_{i=1}^{N} (s_{ij} \cdot p_{ij})$. Equation (12)-(13) is yet appropriate to account in radio resource scheduling problems because it does not realise that the potential total radiation exposure of each individual user is cumulative and depends on the number of the active radios on user j's equipment (e.g. WiFi, Bluetooth, cellular, etc.). In technical terms, given (12)-(13), constraint (8) of problem (1)-(8) can be either expressed as $\Omega_j(f) \cdot \sum_{i=1}^{N} P_j^{rad} \leq SAR^{\text{limit}}$ or $\sum_{i=1}^{N} \left(\Omega_j(f) \cdot P_j^{rad} \right) \leq SAR^{\text{limit}}$. To evaluate appropriateness between the two expressions we track preliminary evidence in [10]-[14] to conclude that for closely spaced antennas it stands

$$\Omega_j(f) \cdot \sum_{i=1}^{N} P_j^{Tx} << \sum_{i=1}^{N} \left(\Omega_j(f) \cdot P_j^{Tx} \right). \tag{14}$$

With equation (14) we intend to convey the hypothesis that SAR estimations (or measurements with lab equipment) taken with more than one transmitter active (corresponding to the left side of (14)) are generally much less than the sum of the SAR measurements taken with each transmitter separately (corresponding to the right side of (14)).

---

[4]The SAR expression in (12)-(13) is valid for the 95th-percentile absorption of adult population standing in the radiating area of the BS's antenna operating between 300MHz and 5GHz [29].

TABLE 1 Summary of variables included in the SAR estimation formula $\Omega_j(f)$ of equations (12)-(13).

Variable	Description
$\Omega_j(f)$	frequency dependent function to express SAR effect based on users' morphology and positions
P^{rad}	radiated power from the BS antenna to the user's body (in W)
$R(f)_{wb/1g,10g}$	frequency dependent ratio of peak spatial SAR over the whole body SAR for 1gr and 10gr of tissue
ω	angular frequency of the BS antenna (in Hz)
Φ_{3dB}	horizontal half-power beam-width of BS antenna (in degree)
L	height of the antenna at the BS (in meter)
δ	distance between outer most point of BS antenna and the box that encloses the antenna (in meter)
$\sigma(f)$	conductivity of the user's tissue-simulating material (in Siemens/meter)
$\rho(f)$	mass density of user's tissue-simulating material (in Kg/m3)
μ	complex magnetic permeability inside the body of the user (in Henry/meter)
ε_0	permittivity of free space given by 8.85×10^{-12} (in Farad/meter)
ε_r	complex relative permittivity at distance r (in Farad/meter)
ε'_r	imaginary part of the complex relative permittivity ε_r (in Farad/meter)
G_A	directivity of the power radiated from the BS antenna (in dB)

This phenomenon is a manifestation of the fact that SAR is a power density measurement, rather than total power measurement, e.g., the numerator in (11) requires a measurement of the squared electric field E^2 in one/ten gram(s) of tissue, whereas the total power is obtained from the squared electric field integrated over all three-dimensional space around the transmitting object. In addition, the quantification of equation (14) is subject to the study in [14], which concludes that using SAR formulas in the form of the left hand side of (14) can bring 3-4dB gain in equivalent transmit power due to multi-channel diversity, while the right hand side of (14) can bring marginal degradations of the overall system performance. In consequence, we can reformulate the $SAR_{j/1g,10g}$ estimation formula in (12) as presented in the left hand side of (14), i.e.,

$$SAR_{j/1g,10g} = \Omega_j(f) \cdot \sum_{i=1}^{N} P_j^{rad} = \Omega_j(f) \cdot \underbrace{\sum_{i=1}^{N} \left(s_{ij} \cdot p_{ij}\right)}_{P_j^{Tx}}. \tag{15}$$

With equations (10) and (15) we can sufficiently describe the radiation exposure constraints (7) and (8) by means of the subcarrier and power optimisation operands s_{ij} and p_{ij} at physical layer, respectively.

4 | JOINT OPTIMAL SUBCARRIER AND POWER ALLOCATION SOLUTION FOR RADIATION-AWARE GREEN COMMUNICATION SYSTEMS

This Section reformulates the resource scheduling problem (1)-(8) using the MPE and SAR expressions in (10) and (15), respectively, to propose the joint optimal policy for green resource scheduling. Notice that by associating the
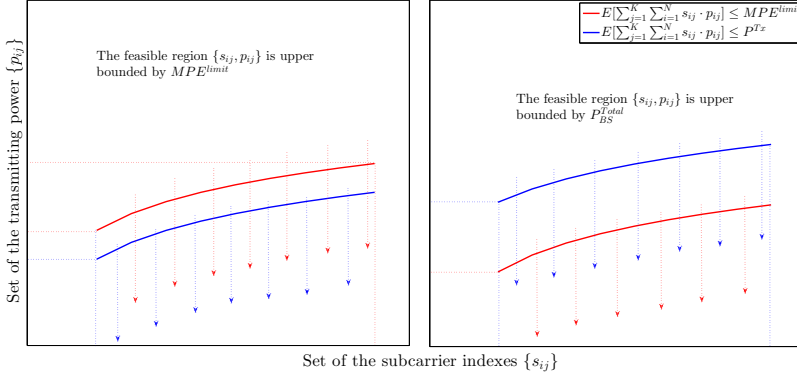
FIGURE 2 Impact of constraints (4) and (10) on the determination of the feasible set $\{s_{ij}, p_{ij}\}$ of problem (1)-(8).

MPE expression (10) with the power constraint (4) of problem (1)-(8), two different upper bounds are outlined with respect to the transmit sum-power P^{Tx}, i.e., $P^{Tx} \leq P_T$ and $P^{Tx} \leq MPE^{\text{limit}'}$. To avoid redundancy, most relevant problems consider bounding the sum-power only using $P^{Tx} \leq MPE^{\text{limit}'}$ assuming that in practice BSs are supplied by tens of watts of power, while the permissible MPE limits are usually sufficiently lower such that $MPE^{\text{limit}'} << P_T$. However, there may be instances where some users can be far enough from the BS's position and the radial distance δ between the BS and the system users can be large enough such that the corresponding MPE-related boundary (10) is larger than the P_T-related boundary (4) . In such cases, the feasible $\{s_{ij}, p_{ij}\}$ region is smaller than the region where $\{s_{ij}, p_{ij}\}$ can be actually determined, thus the optimal solution with respect to s_{ij} and p_{ij} will be suboptimal and performance will be degraded as shown in Figure 2. To include such occasions in our scheduling problem, we bound the transmit sum-power with $P^{Tx} \leq \min \left\{ P_T, MPE^{\text{limit}'} \right\}$, which indicates that the feasible region of $\{s_{ij}, p_{ij}\}$ is dependent dynamically by user positioning with respect to emitting antennas. That way, we reduce complexity of problem (1)-(8) by shrinking two of its rules into single constraint, and simultaneously we ensure maximum protection to users by including both MPE bounds (4) and (10).

4.1 | Reformulation of the Optimisation Problem

The initial problem (1)-(8) is mixed combinatorial with respect to s_{ij} and p_{ij} with impracticable computationally complexity since it has to evaluate K^N combinations to assign the N available subcarriers to the K system users at each transmission frame. To avoid such exponential complexity we tract our problem by relaxing the subcarrier allocation constraints (2) and (3) with the time-sharing factor $\tilde{s}_{ij} \in (0, 1]$, which indicates the portion of time that subcarrier i is assigned to user j during each transmission frame [22]-[24]. Also, we define variable $\tilde{p}_{ij} = p_{ij} \cdot \tilde{s}_{ij} \geq 0$, which indicates the portion of power allocated to user j on subcarrier i during a time-share $\tilde{s}_{ij}$. With the aid of the continuous time-sharing variables $\tilde{s}_{ij}$ and $\tilde{p}_{ij}$, problem (1)-(8) can be reformulated as follows.

$$\min_{\tilde{s}_{ij} \in (0,1], \tilde{p}_{ij} \geq 0} \sum_{j=1}^{K} \sum_{i=1}^{N} \tilde{p}_{ij} \qquad (16)$$

subject to:
$$\sum_{j=1}^{K} \tilde{s}_{ij} \leq 1, \quad \forall i, \qquad (17)$$

$$\tilde{r}_j = \frac{BW}{N} \cdot \sum_{i=1}^{N} \left(\tilde{s}_{ij} \cdot \log_2 \left(1 + \frac{\tilde{p}_{ij} \cdot |h_{ij}|^2}{\tilde{s}_{ij} \cdot \Gamma \cdot \frac{N_0 \cdot BW}{N}} \right) \right) \geq q_j, \quad \forall j, \tag{18}$$

$$\tilde{P}^{Tx} = \sum_{j=1}^{K} \sum_{i=1}^{N} \tilde{p}_{ij} \leq \min \left\{ P_T, MPE^{\text{limit}'} \right\}, \tag{19}$$

$$\Omega_j(f) \cdot \sum_{i=1}^{N} \tilde{p}_{ij} \leq SAR^{\text{limit}}, \quad \forall j. \tag{20}$$

Notice that the reformulated objective (16) with constraints (17), (19), (20) are convex due to their affinity with respect to time-sharing $\tilde{s}_{ij}$ and $\tilde{p}_{ij}$. In addition, function $\tilde{s}_{ij} \cdot \log_2 \left(1 + \frac{\tilde{p}_{ij} \cdot |h_{ij}|^2}{\tilde{s}_{ij} \cdot \Gamma \cdot \frac{N_0 \cdot BW}{N}} \right)$ is concave (i.e. its Hessian matrix is negative definite for $\tilde{s}_{ij}$ and $\tilde{p}_{ij}$ [30]), therefore, constraint (18) is also concave as any positive linear combination of concave functions is concave. In consequence, the $\{\tilde{s}_{ij}, \tilde{p}_{ij}\}$ set determined by the objective and all constraints is concave meaning that the reformulated problem (16)-(20) is concave and there exists a unique optimal solution, which can be obtained in polynomial time.

4.2 | Derivation of Joint Optimal Resource Scheduling Solution

Let us initially set $a_{ij} = \frac{|h_{ij}|^2}{\Gamma \cdot \frac{N_0 \cdot BW}{N}}$ for brevity. The Lagrangian function of problem (16)-(20) is then given by

$$\begin{aligned} L(\{\tilde{s}_{ij}\}, \{\tilde{p}_{ij}\}, \{w_i\}, \lambda, \{q_j\}, \{y_j\}) = & -\sum_{j=1}^{K} \sum_{i=1}^{N} \tilde{p}_{ij} - \omega_i \cdot \left(\sum_{j=1}^{K} \tilde{s}_{ij} - 1 \right) + \\ & \theta_j \cdot \left(\frac{BW}{N} \cdot \sum_{i=1}^{N} \tilde{s}_{ij} \cdot \log_2 \left(1 + \frac{\tilde{p}_{ij} \cdot a_{ij}}{\tilde{s}_{ij}} \right) - q_j \right) - \\ & \lambda \cdot \left(\sum_{j=1}^{K} \sum_{i=1}^{N} \tilde{p}_{ij} - \min\{P_T, MPE^{\text{limit}'}\} \right) - \\ & \psi_j \cdot \left(\Omega_j(f) \cdot \sum_{i=1}^{N} \tilde{p}_{ij} - SAR^{\text{limit}} \right) \end{aligned}, \tag{21}$$

where ω_i, $\theta_j \geq 0$, $\lambda \geq 0$ and $\psi_j \geq 0$ denote the Lagrangian multipliers for the constraints (17), (18), (19) and (20), respectively. The *Karush-Kuhn-Tucker* (KKT) conditions yield

$$\frac{\partial L\left(\{\tilde{s}_{ij}\}, \{\tilde{p}_{ij}\}, \{\omega_i\}, \lambda, \{\theta_j\}, \{\psi_j\}\right)}{\partial \tilde{p}_{ij}} \Bigg|_{\left(\tilde{p}_{ij}, \tilde{s}_{ij}, \omega_i, \lambda, \theta_j, \psi_j\right) = \left(\tilde{p}_{ij}^*, \tilde{s}_{ij}^*, \omega_i^*, \lambda^*, \theta_j^*, \psi_j^*\right)} \begin{cases} = 0 \text{ if } \tilde{p}_{ij}^* > 0 \\ < 0 \text{ if } \tilde{p}_{ij}^* = 0 \end{cases}, \tag{22}$$

$$\frac{\partial L\left(\{\tilde{s}_{ij}\}, \{\tilde{p}_{ij}\}, \{\omega_i\}, \lambda, \{\theta_j\}, \{\psi_j\}\right)}{\partial \tilde{s}_{ij}^*} \Bigg|_{\left(\tilde{p}_{ij}, \tilde{s}_{ij}, \omega_i, \lambda, \theta_j, \psi_j\right) = \left(\tilde{p}_{ij}^*, \tilde{s}_{ij}^*, \omega_i^*, \lambda^*, \theta_j^*, \psi_j^*\right)} \begin{cases} < 0 \text{ if } \tilde{s}_{ij}^* = 0 \\ = 0 \text{ if } 0 < \tilde{s}_{ij}^* < 1 \\ > 0 \text{ if } \tilde{s}_{ij}^* = 1 \end{cases}, \tag{23}$$

$$\lambda^* \cdot \left(\sum_{j=1}^{K} \sum_{i=1}^{N} \tilde{p}_{ij}^* - \min \left\{ P_T, MPE^{\text{limit}'} \right\} \right) = 0, \tag{24}$$

$$\theta_j^* \cdot \left(\frac{BW}{N} \cdot \sum_{i=1}^{N} \tilde{s}_{ij}^* \cdot \log_2 \left(1 + \frac{\tilde{p}_{ij}^* \cdot a_{ij}}{\tilde{s}_{ij}^*} \right) - q_j \right) = 0, \tag{25}$$

$$\psi_j^* \cdot \left(\Omega_j(f) \cdot \sum_{i=1}^{N} \tilde{p}_{ij}^* - SAR^{\text{limit}} \right) = 0. \tag{26}$$

By differentiating the Lagrangian in (21) with respect to $\bar{p}_{ij}$ and substituting the result into the KKT condition (22) we obtain the optimal instantaneous power allocated to subcarrier i for user j as

$$\bar{p}_{ij}^* = \frac{\tilde{s}_{ij}^*}{a_{ij}} \cdot \left(\frac{\theta_j^*}{\lambda^* + \psi_j^* \cdot \Omega_j(f) + 1} \cdot \frac{BW \cdot a_{ij}}{\ln 2 \cdot N} - 1 \right)^+, \tag{27}$$

with $(x)^+ \triangleq \max(0, x)$. Furthermore, we calculate the optimal subcarrier indexing by taking the partial derivative of the Lagrangian in (21) with respect to $\tilde{s}_{ij}^*$, which yields

$$\frac{\partial L\left(\{\tilde{s}_{ij}\}, \{\bar{p}_{ij}\}, \{\omega_i\}, \lambda, \{\theta_j\}, \{\psi_j\} \right)}{\partial \tilde{s}_{ij}^*} \Bigg|_{\left(\bar{p}_{ij}, \tilde{s}_{ij}, \omega_i, \lambda, \theta_j, \psi_j \right) = \left(\bar{p}_{ij}^*, \tilde{s}_{ij}^*, \omega_i^*, \lambda^*, \theta_j^*, \psi_j^* \right)} =$$
$$\theta_j^* \cdot \frac{BW}{N} \left(\log_2 \left(1 + \frac{\bar{p}_{ij}^* \cdot a_{ij}}{\tilde{s}_{ij}^*} \right) - \frac{\bar{p}_{ij}^* \cdot a_{ij}}{\ln 2 \cdot \tilde{s}_{ij}^* \cdot \left(1 + \frac{\bar{p}_{ij}^* \cdot a_{ij}}{\tilde{s}_{ij}^*} \right)} \right) - \omega_i^* = 0 \tag{28}$$

By substituting the optimal power allocation (27) into (28) and applying the KKT condition (23), we obtain

$$H_{ij}\left(Y_j^* \right) - \omega_i^* \begin{cases} < 0 \text{ if } \tilde{s}_{ij}^* = 0 \\ = 0 \text{ if } 0 < \tilde{s}_{ij}^* < 1 \quad \Rightarrow, \\ > 0 \text{ if } \tilde{s}_{ij}^* = 1 \end{cases} \tag{29}$$

$$\tilde{s}_{ij}^* = \begin{cases} 0 \text{ if } H_{ij}(Y_j) < \omega_i \\ 1 \text{ if } H_{ij}(Y_j) > \omega_i \\ \in (0, 1) \text{ if } H_{ij}(Y_j) = \omega_i \end{cases}, \tag{30}$$

where function $H_{ij}\left(Y_j^* \right)$ is given by

$$H_{ij}\left(Y_j^* \right) = \frac{BW}{N} \cdot \left\{ \theta_j^* \cdot \left(\log_2 \left(\frac{BW \cdot Y_j^* \cdot a_{ij}}{\ln 2 \cdot N} \right)^+ + \frac{1}{\ln 2} \cdot \left(\frac{\ln 2 \cdot N}{BW \cdot Y_j^* \cdot a_{ij}} - 1 \right)^+ \right) \right\}. \tag{31}$$

Recalling constraint (17), which bounds each subcarrier to be allocated to single user only, we can decouple the optimal subcarrier assignment into N independent problems using relations (29)-(31), i.e., the user with the largest $H_{ij}\left(Y_j^* \right)$ can use subcarrier i. Having calculated the optimal power and subcarrier indexing in (27) and (29)-(30), respectively, we can readily define the joint optimal resource allocation solution in the following Theorem 1.

Theorem 1 *The optimal power allocation policy of the convex optimisation problem* (16)-(20) *is obtained as* $\mathcal{P}_{N \times K}\left[\mathcal{S}_{N \times K} \right] = \left[\bar{p}_{ij}^* \right]$, *where* $\bar{p}_{ij}^*$ *is optimal instantaneous transmit power allocated to user j on subcarrier i given by* (27). *The corresponding optimal subcarrier allocation policy is obtained as* $\mathcal{S}_{N \times K}\left[\mathcal{P}_{N \times K} \right] = \left[\tilde{s}_{ij}^* \right]$ *with individual element* $\tilde{s}_{ij}^*$ *the optimal subcarrier allocation index given by the linear search*

$$\begin{aligned} &\text{For } i = 1 : N \\ &\quad j^* = \arg\max_{j \in \{1, \ldots, K\}} H_{ij}\left(Y_j^* \right) \\ &\quad \tilde{s}_{ij}^* = \begin{cases} 1, \ j = j^* \\ 0, \ \text{otherwise} \end{cases} \end{aligned} \tag{32}$$

where j^* is the optimal user index with function $H_{ij}\left(Y_j^*\right)$ defined in (31).

Next Section discusses some key properties on the of the implementation process and complexity of the proposed optimal policy in Theorem 1.

5 | PROPERTIES AND IMPLEMENTATION PROCESS OF THE PROPOSED SO-LUTION

The optimal power allocation policy (27) follows the standard water-filling approach, except that the optimal power $\bar{\rho}_{ij}^*$ can be allocated for $\bar{s}_{ij}^*$ fraction of time. During this time, more power is to be allocated to the subcarriers with higher SNR a_{ij} than others, and vice versa. Moreover, by substituting (27) into the KKT condition (25) and recalling $\vartheta_j^* \neq 0$ we obtain the closed-form expression for the water-level of each user as

$$\tilde{Y}_j^* = \left[\frac{\ln 2 \cdot N \cdot 2^{\frac{N \cdot q_j}{BW}}}{BW \times \prod_{i=1}^{N'} \left(\frac{\ln 2 \cdot N \cdot \left(\lambda^* + \psi_j^* \cdot \Omega_j(f) + 1 \right)}{BW \cdot \theta_j^*} \right)^{\bar{s}_{ij}^*}} \right]^{\frac{1}{\sum_{i=1}^{N'} \bar{s}_{ij}^*}}, \tag{33}$$

where $N' \subset N$ is the set of the subcarriers assigned to user j. More precisely, the water-level of each system user in (33) can be used to equalise the subcarriers during the operation of the proposed optimal strategy. Variable Y_j represents the power level of each user j, where each subcarrier has to be amplified compensating for the user's channel conditions. Therefore, the water-level Y_j can be regularly used to represent the signal quality as well as the efficiency of each user, e.g., low water-levels (before optimisation) are issued by users in bad channel conditions and therefore, to users which demand more system resources than other users. Note that unlike traditional water-filling approach, the proposed water-level $\tilde{Y}_j^*$ in (33) is dynamic, which means that the water-level is not constant but changes according to user requirements and characteristics. For instance, multiplier θ_j^* depends on the $j-$th user QoS demands, while ψ_j^* and λ^* depend on its SAR^{limit} and $\min\left\{P_T, MPE^{\text{limit}'}\right\}$ value, respectively. Large θ_j^* means that $j-$th user has high QoS demands and it is expected its corresponding SAR multiplier ψ_j^* to be relatively small meaning that exposure to radiation is high when QoS is high, and vice versa. In addition, large λ^* indicates that the overall radiated power bound is small and therefore, BS transmits at relatively low power, and vice versa. In consequence, using (33) we can evaluate if all three constraints (18), (19) and (20) (which regard the minimum QoS requirements, MPE and SAR exposure levels of each user, respectively) have been completely satisfied for each user[5]. It follows that for a given set of water levels $\left\{Y_0^*, ..., Y_j^*, ..., Y_K^*\right\}$, or equivalently, a given set of Lagrangian multipliers $\left\{\lambda^*, \left\{\theta_j^*\right\}, \left\{\psi_j^*\right\}\right\}$, we can determine the optimal subcarrier allocation using the search in (32).

Furthermore, function $H_{ij}\left(Y_j^*\right)$ in (32) plays key role in acquiring the joint optimal solution. For instance, it can be verified that $H_{ij}\left(Y_j^*\right)$ monotonically increases with respect to $a_{ij}(h_{ij})$ meaning that for each subcarrier, the user with good channel conditions (large SNR) is more likely to be assigned this subcarrier. Also, $H_{ij}\left(Y_j^*\right)$ is non-decreasing function with respect to Y_j^*, which means that when the water-level Y_j^* of user j increases, this user has higher chances to occupy more subcarriers than others.

---

[5] We show in Appendix that the expression of the water-level $\tilde{Y}_j^*$ in (33) is particularly useful for the initialisation of the implementation algorithm, where the QoS and SAR targets of each user must be guaranteed all the time.

Based on the aforementioned observations, we propose an iterative algorithm, which can obtain the optimal water-levels Y_j^* and determine the corresponding power and subcarrier assignments $\tilde{p}_{ij}^*$ and $\tilde{s}_{ij}^*$ in (27) and Theorem 1 by simultaneously satisfying the QoS, MPE and SAR constraints (18), (19) and (20), respectively.

Implementation process of the proposed algorithm

The proposed algorithm aims to obtain the set of optimal water levels $\left\{Y_1^*, ..., Y_j^*, ..., Y_K^*\right\}$ using three nested loops. One outer loop is used to vary λ such that the total MPE constraint (19) is fulfilled. Two inner loops search for the sets of $\{\theta_j, ..., \theta_K\}$ and $\{\psi_j, ..., \psi_K\}$ to satisfy the minimum QoS requirement (18) and the SAR limit (20) of each user, respectively. At each iteration n, the algorithm determines the optimal $\tilde{s}_{ij}^*$ for all i and j at the given values of $\left(\lambda^{(n)}, \left\{\psi_j^{(n)}\right\}, \left\{\theta_j^{(n)}\right\}\right)$. The proposed algorithm guarantees the constant-rate transmission of system users in probabilistic manner since the MPE value at the BS is fixed and finite. Also, the service is said to be in outage if any of the minimum QoS requirements cannot be satisfied. This is because upon excluding the QoS constraint (18), the MPE and SAR constraints (19) and (20), respectively will be always satisfied, e.g., $\left\{\tilde{p}_{ij}^*\right\} \rightarrow 0$ and therefore, the feasibility of the proposed algorithm is related to the condition that $MPE^{\text{limit}'} \geq P_{\min}$, where $P_{\min}$ is the minimum total power needed to support all users' QoS requirements. For the ease of presentation, the pseudo-code of the proposed algorithm is presented in Appendix including comments for the allocation mechanism of each loop.

Computational complexity of the proposed algorithm

The computational complexity of the proposed algorithm lies in the number of iterations needed to update λ in the outer loop and the number of iterations to update $\{\theta_j, \psi_j\}$ for each λ in the two inner loops. Each λ is evaluated using the bisection method, therefore the number of iterations required to achieve ε-optimality, i.e., $\lambda - \lambda^* = \varepsilon$, is on the order of $O\left(\log_2\left(1/\varepsilon\right)\right)$. At each of the two inner loops, the bisection is also used to seek and update the sets of $\{\theta_j\}$ and $\{\psi_j\}$, thus the algorithm requires $\log_2\left(1/\varepsilon\right)$ iterations for each loop. In addition, at each iteration the $\tilde{s}_{ij}^*$ and $\tilde{p}_{ij}^*$ are obtained $N \cdot K$ times, i.e., for all N subcarriers and K users. Consequently, the total complexity of the proposed algorithm (including all three loops) is on the order of $O\left(N \cdot K \cdot \log_2\left(1/\varepsilon\right)\right)$.

6 | EVALUATIONS ON GREEN PERFORMANCE

This section carries out simulations to examine the green performance of the proposed optimal solution, namely MPE-SAR-aware transmit power minimisation scheduler (MSminPx). Particularly, we compare MSminPx with relevant QoS-aware scheduling schemes of minimum power (minPx) [25], maximal rate (maxRx) [22], [26] and minimum power with fixed subcarrier assignment (minPx-Fixed) [27] scheduling. For the fair comparisons, we set all schemes to use same hardware equipment (e.g. antenna positioning and geometry, ferrite materials or metamaterials, etc.) such that the potential radiation reduction due to hardware enchantments is same for all schedulers. Also, to keep consistency among comparisons we adopt in Table 2 the similar simulation setting with minPx, maxRx and minPx-Fixed approaches in [22], [25]- [27], which are based on the LTE wireless standard. Furthermore, we consider 6-tap multipath fading downlink channels with exponential-decay power-delay profiles, 20MHz sampling frequency and 50ns RMS delay spread. Channels of different users are independent, while the path losses from the BS to all users are the same. The average channel gain on each subcarrier is normalised with $P_T/(BW \cdot N_0)$ to denote the system (total) transmit SNR.

TABLE 2 Simulation settings in accordance to the relative studies [22], [25]-[27] and the LTE wireless standard.

Variable	Value		Variable	Value
BER	10^{-6}		Φ_{3dB}	66 degrees
P_T	50 W		$R_{wb/1gr}$	0.6
N_0	1		G_A	0.19 dB
MPE^{limit}	1 mW/cm^2 0.0833 mW/cm^2		d	5 cm
Total QoS	13 Mbps 19 Mbps		$C(f)$	6.3
SAR_j^{limit}	1.6 W/Kg per 1gr of tissue 2.0 W/Kg per 10gr of tissue		Γ	8.14 dBm
$\{q_1, q_2, q_3, q_4, q_5, q_6, q_7, q_8\}$	$\{0.75, 1.0, 1.25, 1.5, 1.75, 2.0, 2.25, 2.5\}$ Mbps $\{1.5, 1.75, 2.0, 2.25, 2.5, 2.75, 3.0, 3.25\}$		BW	80 KHz
$\{\Omega_1, \Omega_2, \Omega_3, \Omega_4, \Omega_5, \Omega_6, \Omega_7, \Omega_8\}$	$\{4.47, 2.23, 1.49, 0.89, 0.56, 0.45, 0.37, 0.29\}$		K	16
$R_{wb/1gr}$	0.6 for 300MHz $\leq$ f $\leq$ 2.5GHz 0.3 for 2.5GHz $\leq$ f $\leq$ 5GHz		N	64
$R_{wb/10gr}$	1.5 for 300MHz $\leq$ f $\leq$ 2.5GHz 1 for 2.5GHz $\leq$ f $\leq$ 5GHz		L	20 m

6.1 | Simulation Results

In Figure 3, we compare the total transmit power and throughput versus SNR of the considered schemes[6]. We observe that as SNR increases, the proposed MSminPx performs almost identically with minPx in terms of both radiated power and throughput in Figure 3a and Figure 3b, respectively. This is because the impact of the QoS constraint (18) on each scheduling decision $\{\bar{s}_{ij}^*, \bar{p}_{ij}^*\}$ in (27) and (32) is higher than the impact of MPE and SAR constraints (19) and (20), respectively, therefore MSminPx performs similarly to conventional minPx. On the other hand, the fixed subcarrier distribution of minPx-fixed limits resource scheduling flexibility thus, degrades power and throughput performances, while maxRx acts purely opportunistic achieving the highest throughput among the considered schemes. However, upon examining the corresponding to each scheme MPE and SAR radiation levels in Figure 4, we see that the pure opportunistic scheduling of maxRx does not comprise safest solution exceeding both MPE and SAR thresholds, thus exposing users to potentially unsafe levels of radiation. In contrary, MSminPx, minPx and minPx-fixed, which consider power minimisation, can sufficiently conform to the permissible WHO/NRPB radiation levels of exposure even with fixed subcarrier distributions. Consequently, the choice of optimisation objective in scheduling problems plays key role to promote radiation awareness, while keeping power and throughput performances at adequate levels.

Figure 5-Figure 9 set stricter radiation exposure limits and higher user QoS requirements than Figure 3 and Figure 4 to validate each scheme's boundary performances[7]. Particularly, in Figure 5a and Figure 5b we observe that the performances of minPx, maxRx and minPx-fixed are analogous to the previous experiments except that they have

---

[6] For the experiments in Figure 3-Figure 4, we assume that (i) all users are far enough from the BS such that the MPE limit is sufficiently large, (e.g. $MPE^{\text{limit}} = 1$ mW/cm^2, $MPE^{\text{limit}'} \geq P_T$) and (ii) each user can tolerate the maximum permissible WHO/NRPB limit for SAR of 1.6 W/Kg per 1gr.

[7] For the experiments in Figure 5-Figure 9, we assume that (i) all users are positioned in relatively close distances from the BS, e.g., the minimum radial distance of each user is set $\delta = 20$ meters (recall Figure 1) such that MPE^{limit} is decreased from 1 mW/cm^2 to 0.0833 mW/cm^2 [28], (ii) the maximum SAR^{limit} a user can tolerate is decreased from 1.6 W/Kg to 0.60 W/Kg per 1gr of tissue and (iii) the total required QoS is 19 Mbps with each user's individual QoS requirement given in Table 2.
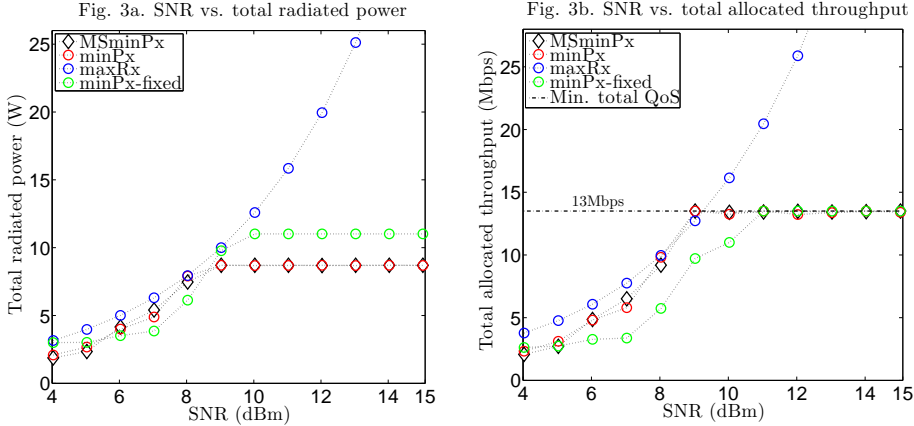
FIGURE 3 Total radiated power and total allocated throughput versus SNR considering MPE^{limit} = 1.0 mW/cm^2, SAR^{limit} = 1.6 W/Kg and minimum user QoS requirement q_j = 13 Mbps.

been up-scaled according to the increase of the required QoS. On the other hand, the proposed MSminPx achieves lowest radiating power by providing 3Mbps lower throughput in average than the minimum required. This is because the determination $\left\{\tilde{s}_{ij}^*, \tilde{p}_{ij}^*\right\}$ region in MSminPx is the conjunction of $2K+1$ regions dependent on (i) the MPE constraint (19), (ii) each of the K in total QoS constraints (18) and (iii) each of the K in total SAR constraints (20). Instead, the corresponding $\left\{\tilde{s}_{ij}^*, \tilde{p}_{ij}^*\right\}$ region in minPx, maxRx and minPx-fixed is dependent on the conjunction of the K in total QoS constraints only meaning that the feasible space where MSminPx seeks for the optimal solutions is smaller than the feasible space determined by the traditional scheduling approaches, and thus MSminPx throughput performance degrades. Such throughput degradation is inevitable in radiation-aware scheduling solutions, which aim to balance the trade-off between QoS and exposure to radiation. For instance, Figure 6a shows that although the throughout cost,
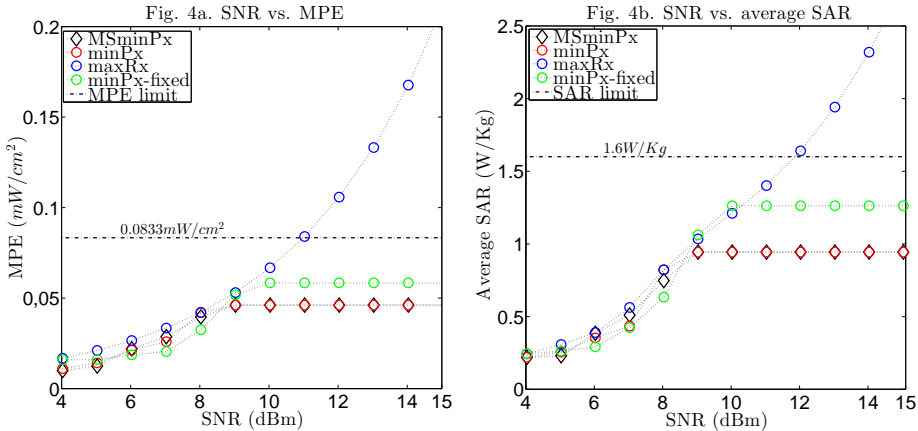

FIGURE 4 MPE and average SAR versus system SNR considering MPE^{limit} = 1.0 mW/cm^2, SAR^{limit} = 1.6 W/Kg and minimum user QoS requirement q_j = 13 Mbps.

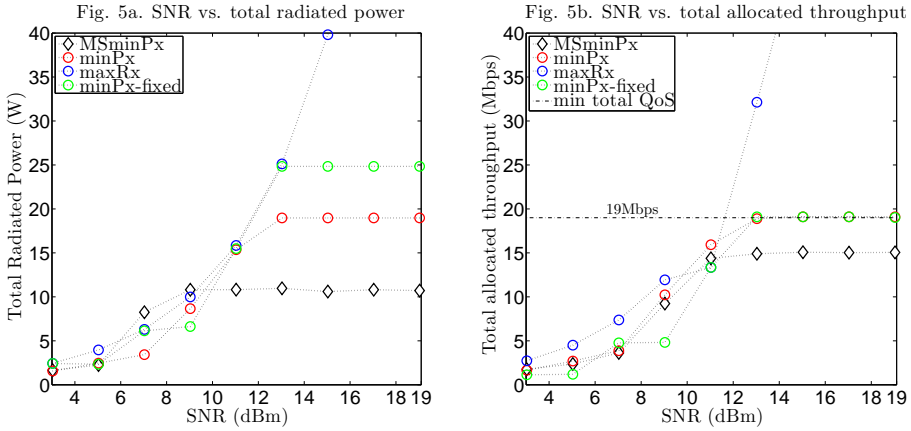**FIGURE 5** Total radiated power and total allocated throughput versus SNR under MPE^{limit} = 0.0833 mW/cm^2, SAR^{limit} = 0.6 W/Kg and minimum user QoS requirement q_j = 19 Mbps.

MSminPx can retain the MPE below its lowest threshold (e.g. 0.0833 mW/cm^2) within the whole SNR region and for all users, while minPx, maxRx and minPx-fixed expose users to much higher MPE-oriented radiation (e.g. 0.145 mW/cm^2). Similarly, in Figure 6b MSminPx preserves average user SAR below its lower threshold (e.g. 0.60 W/Kg), while the average SAR level in minPx, maxRx and minPx-fixed is considerably higher (e.g. it exceeds the 3.20 W/Kg, especially under high SNR).

To further examine the green performance of each considered scheme we illustrate in Figure 7 the MPE and SAR violation percentages versus the SNR. Particularly, we see that by using MSminPx scheduling, MPE radiation reaches the 44% of its maximum limit (i.e. MPE^{limit} = 0.0833 mW/cm^2), while SAR level reaches the 78% of its hiest threshold (i.e. SAR^{limit} = 0.60 W/Kg) as shown in Figure 7a and in Figure 7b, respectively. The corresponding radiation
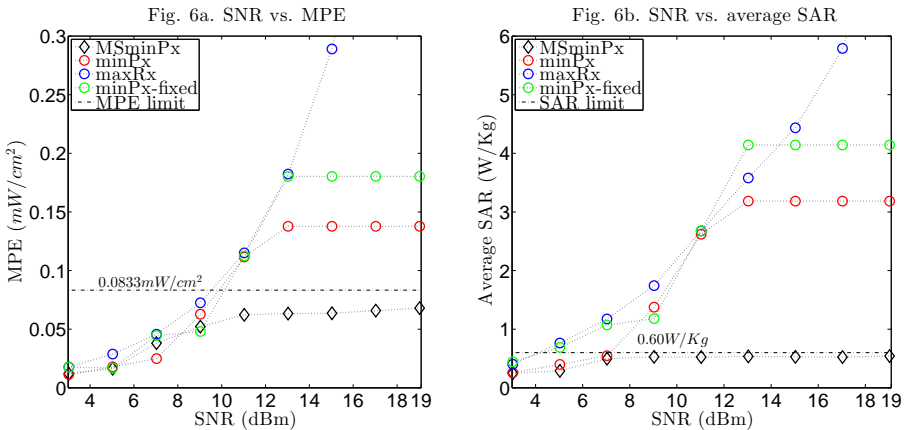

FIGURE 6 Total radiated power and total allocated throughput versus SNR under MPE^{limit} = 0.0833 mW/cm^2, SAR^{limit} = 0.6 W/Kg and minimum user QoS requirement q_j = 19 Mbps.

Fig. 7a. SNR vs. violation of MPE limit

Fig. 7b. SNR vs. violation of SAR limit

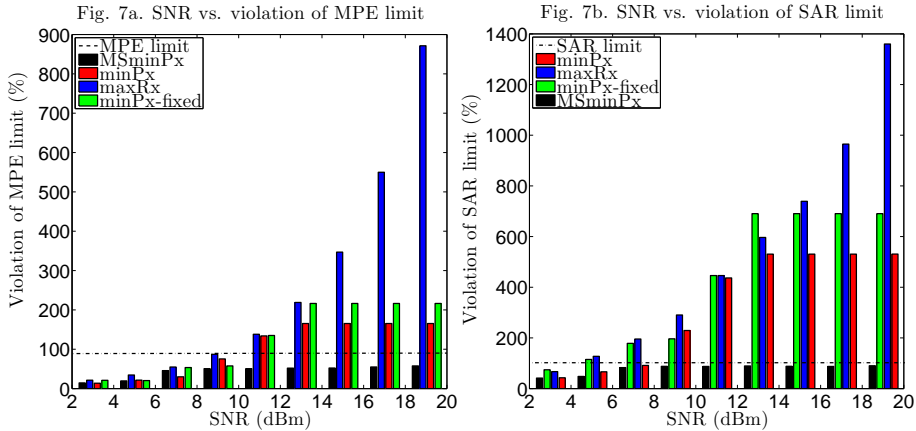**FIGURE 7** Violation of SAR and MPE limits versus SNR under MPE^{limit} = 0.0833 mW/cm^2, SAR^{limit} = 0.6 W/Kg and minimum user QoS requirement q_j = 19 Mbps.

levels for minPx, maxRx and minPx-fixed are notably higher than the proposed MSminPx, i.e., 104%, 258% and 128% higher MPE and 332%, 532% and 419% higher SAR levels. To justify the MPE and SAR violation in traditional minPx, maxRx and minPx-fixed approaches, Figure 8 provides a detailed view of the resultant SAR for each user. Indeed, the SAR level of user 3 and user 7 (which have similar QoS but better channel conditions than others) is particularly high, especially when using opportunistic maxRx scheduling. In addition, Figure 9 examines the trade-off between throughput performance and radiation exposure for SNR = 14 dBm. It can be seen that the proposed MSminPx satisfies the minimum QoS requirement of each user resulting with particularly low SAR levels of 0.75 W/Kg, while it outperforms minPx and minPx-fixed by 0.85 Mbps and 1.08 Mbps, which corresponds to 2.12 W and 3.78 W of power gain, respectively. This is because traditional power minimisation problems take their optimal scheduling deci-

Fig. 8a. MSminPx scheduling

Fig. 8b. minPx scheduling
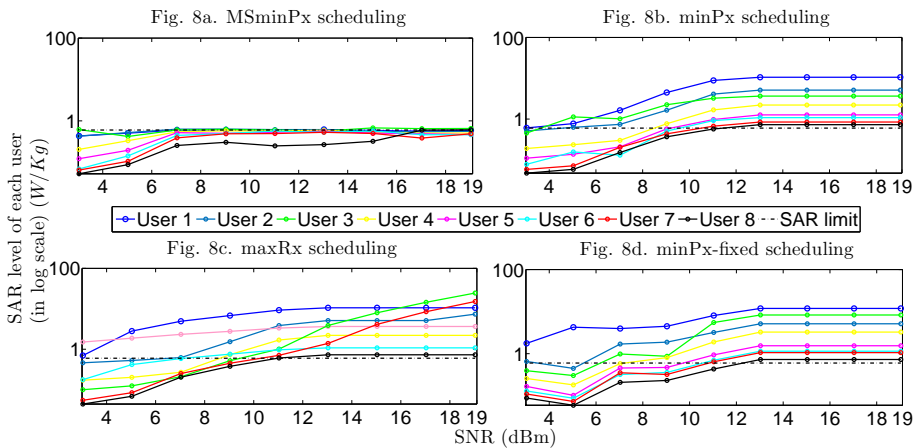
Fig. 8c. maxRx scheduling

Fig. 8d. minPx-fixed scheduling

FIGURE 8 SAR level of each user versus SNR under MPE^{limit} = 0.0833 mW/cm^2, SAR^{limit} = 0.6 W/Kg and minimum user QoS requirement q_j = 19 Mbps.

Fig. 9. SAR limit vs. total allocated throughput

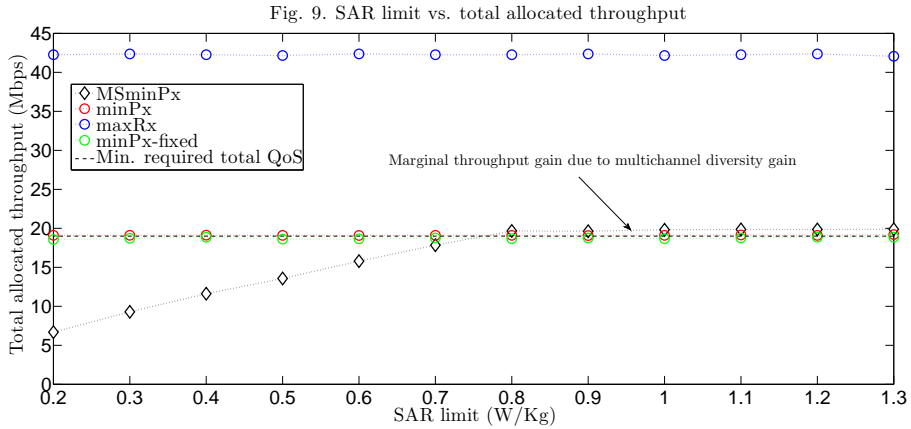**FIGURE 9** SAR limit versus total allocated throughput under $MPE^{\text{limit}} = 0.0833$ mW/cm^2, $SAR^{\text{limit}} = 0.6$ W/Kg and minimum user QoS requirement $q_j = 19$ Mbps.

sions considering the boundary of the total transmit power constraint (such as constraint (4)), while the boundaries in the radiation-aware MSminPx scheduling depend on either the total transmit power constraint (19) or the set of the individual user SAR constraint (20), which potentially provides more flexibility to allocate the power resources.

In summary, Figure 3 – Figure 9 show that by using traditional scheduling approach, the exposure to radiation of users with high QoS can exceed the FCC/CENELEC safety thresholds, while by constraining the problem with respect to MPE and SAR limits (as done in (19) and (20), respectively) the radiation levels can drop to much lower levels with the required minimum QoS provision.

7 | CONCLUSION

In this paper, we investigated electromagnetic radiation-aware radio resource scheduling mechanisms towards future generation green wireless communication systems. Specifically, two main radiation exposure metrics, MPE and SAR are considered in the resource scheduling problem to minimise the transmit power levels such that the exposure levels to radiation are below the WHO/NRPB safety standards [31], while satisfying users' minimum QoS requirements. Novel radio resource scheduling mechanisms are proposed and the optimal solutions are obtained, which can jointly perform dynamic subcarrier allocation and adaptive power management according to each user's channel conditions, physical anatomy and QoS demands. Our simulation results demonstrated the effectiveness of the proposed mechanisms, which can be used as key paradigm towards developing more sophisticated solutions for next-generation wireless communication systems that can prevent public heath from potential ill effects of radiation exposure.

Appendix

The Appendix is to summarise and discuss the algorithmic process that implements the proposed solution of joint optimal subcarrier and transmit power scheduling for green radios.

In Figure 10 and Table 3 we provide the block diagram and the pseudo-code of the implementation process, respectively. We see that in the main function (outer loop) the algorithm uses the closed-form expression of the

TABLE 3 Pseudo-code of the implementation process for the proposed scheduling algorithm.

|	
1.	**Main function:** *Outer loop - Subcarrier and Power Allocations*
2.	**Phase 1.** *Initialisation of* $\{Y_1, ..., Y_K\}$
3.	set arbitrary values $\lambda^{(0)}$, $\psi_j^{(0)}$ and $\theta_j^{(0)}$, $\forall j$ for λ, ψ_j and θ_j, respectively, with $n = 0, ..., \infty$ the iteration index
4.	compute the initial $\left\{ Y_j^{(0)} \left(\lambda^{(0)}, \left\{ \psi_j^{(0)} \right\}, \left\{ \theta_j^{(0)} \right\} \right) \right\}$, $\forall j$ and $\tilde{s}_{ij} \left(Y_j^{(0)} \right)$, $\forall i, j$ using (27) and (32)
5.	**Phase 2.** *Update* $\left\{ Y_1^{(0)}, ..., Y_K^{(0)} \right\}$ *such that the MPE constraint is satisfied*
6.	Step 1) compute $\bar{p}_j \left(\tilde{s}_{ij} \left(Y_j^{(0)} \right) \right) = \sum_{i=1}^N \left(\frac{\tilde{s}_{ij^*}^{(0)}}{a_{ij^*}} \cdot \left[Y_j^{(0)} \cdot \frac{BW \cdot a_{ij^*}}{\ln 2 \cdot N} - 1 \right]^+ \right)$, $\forall j$, $P^{Tx} = \sum_{j=1}^K \sum_{i=1}^N \bar{p}_j \left(Y_j^{(0)} \right)$
7.	Step 2) if $P^{Tx} \left(Y_j^{(0)} \right) > MPE^{\text{limit}'}$ *(Power exceeds the MPE limit)*
8.	$\lambda_{LB}^{(0)} = \delta$, where $(\cdot)_{LB}$ to denote the lower bound of a quantity and δ a small number $\lambda_{UB}^{(0)} = \Delta$, where $(\cdot)_{UB}$ to denote the upper bound of a quantity and Δ a large number
9.	repeat *Step 1*
10.	else go to *Step 3*
11.	Step 3) else if $P^{Tx} \left(Y_j^{(0)} \right) < MPE^{\text{limit}'}$ *(Power not totally exploited)*
12.	set $\lambda_{UB}^{(0)} = \delta$
13.	Step 4) update $\lambda^{(n)} = \frac{\lambda_{UB}^{(0)} + \lambda_{LB}^{(0)}}{2}$
14.	compute $\left\{ Y_j^{(n)} \left(\lambda^{(n)}, \left\{ \psi_j^{(0)} \right\}, \left\{ \theta_j^{(0)} \right\} \right) \right\}$ using (33) and $\bar{p}_j \left(\tilde{s}_{ij} \left(Y_j^{(n)} \right) \right)$
15.	if $P^{Tx} \left(Y_j^{(n)} \right) > MPE^{\text{limit}'}$, $\lambda_{LB}^{(0)} \to \delta$
16.	else if $P^{Tx} \left(Y_j^{(n)} \right) < MPE^{\text{limit}'}$, $\lambda_{UB}^{(0)} \to \delta$
17.	repeat *Step 4* until $P_{BS}^{rad} \left(Y_j^{(n)} \right) = B$
18.	**Function:** *Inner loops*
19.	**Phase 3.** *Update* $\left\{ Y_1^{(n)}, ..., Y_K^{(n)} \right\}$ *such that the QoS constraint is satisfied for each user*
20.	Step 5) for each $i = 1, ..., N$
21.	compute $H_{ij} \left(Y^{(n)} \left(\lambda^{(n)}, \left\{ \psi_j^{(0)} \right\}, \left\{ \theta_j^{(0)} \right\} \right) \right)$, $\forall i, j$ using (31)
22.	obtain j^* and $\tilde{s}_{ij^*}^{(n)}$ using *Theorem 1*.
23.	Step 6) for each $j = 1, ..., K$
24.	compute $r_j \left(\tilde{s}_{ij^*}^{(n)} \left(Y_j^{(n)} \right) \right) = \frac{BW}{N} \cdot \sum_{i=1}^N \left(\tilde{s}_{ij^*}^{(n)} \cdot \left[\log_2 \left(Y_j^{(n)} \cdot \frac{BW \cdot a_{ij}}{\ln 2 \cdot N} \right) \right]^+ \right)$, $\forall j$
25.	Step 7) find j^* with $r_{j^*} < q_{j^*}$ and $r_{j^*} - q_{j^*} \le r_j - q_j$ for all $1 \le j \le K$
26.	while $r_{j^*} \left(\tilde{s}_{ij^*}^{(n)} \left(Y_j^{(n)} \right) \right) < q_{j^*}$ for the found j^*
27.	set $\left\{ \theta_{j^*}^{(0)} \right\}_{LB} = \delta$, $\left\{ \theta_{j^*}^{(0)} \right\}_{UB} = \Delta$
28.	update $\theta_{j^*}^{(0)} \to \theta_{j^*}^{(n)}$ with the bisection method (similar to *Step 4*)
29.	compute $\left\{ Y_{j^*}^{(n+1)} \left(\lambda^{(n)}, \left\{ \psi_j^{(0)} \right\}, \left\{ \theta_{j^*}^{(n)} \right\} \right) \right\}$, $\forall j$ using (33)
30.	obtain $\tilde{s}_{ij} \left(Y_{j^*}^{(n+1)} \right)$, $\forall i, j$ using (30) and $r_j \left(\tilde{s}_{ij} \left(Y_{j^*}^{(n+1)} \right) \right)$ using the equation in *line 24*
31.	repeat *Step 7* until $r_{j^*} \left(\tilde{s}_{ij^*} \left(Y_{j^*}^{(n+1)} \right) \right) = q_{j^*}$ for all $j = 1, ..., K$
32.	**Phase 4.** *Update* $\left\{ Y_1^{(n+1)}, ..., Y_K^{(n+1)} \right\}$ *such that the SAR constraint is satisfied for each user*
33.	Step 8) compute $\bar{p}_{j^*} \left(\tilde{s}_{ij^*} \left(Y_{j^*}^{(n+1)} \right) \right) = \sum_{i=1}^N \left(\frac{\tilde{s}_{ij^*}}{a_{ij^*}} \cdot \left[Y_{j^*}^{(n+1)} \cdot \frac{BW \cdot a_{ij^*}}{\ln 2 \cdot N} - 1 \right]^+ \right)$
34.	if $\Omega_{j^*} \cdot \bar{p}_{j^*} \left(\tilde{s}_{ij^*} \left(Y_{j^*}^{(n+1)} \right) \right) \le SAR^{\text{limit}}$ for the found j^*(*SAR is not violated - QoS, MPE are satisfied too*)
35.	*Define optimal Lagrange multipliers:* $\lambda^{(n)} \to \lambda^*$, $\psi_j^{(0)} \to \psi_j^*$, $\theta_j^{(n)} \to \theta_j^*$ *Define optimal subcarrier and power allocations:* $\bar{p}_{j^*} \left(\tilde{s}_{ij^*} \left(Y_{j^*}^{(n+1)} \right) \right) \to \bar{p}_{ij}^*$, $\tilde{s}_{ij^*} \left(Y_{j^*}^{(n+1)} \right) \to \tilde{s}_{ij}^* \forall i, j$
36.	else if $\Omega_{j^*} \cdot p_{j^*} \left(\tilde{s}_{ij^*} \left(Y_{j^*}^{(n+1)} \right) \right) > SAR^{\text{limit}}$ for the found j^* (*SAR is violated, while QoS, MPE are satisfied*)
37.	set $\left\{ \psi_{j^*}^{(0)} \right\}_{LB} = \delta$, $\left\{ \psi_{j^*}^{(0)} \right\}_{UB} = \Delta$
38.	update $\psi_{j^*}^{(0)} \to \psi_{j^*}^{(n)}$ with the bisection method (similar to *Step 4*)
39.	compute $Y_{j^*}^{(n+2)} \left(\lambda^{(n)}, \left\{ \psi_{j^*}^{(n)} \right\}, \left\{ \theta_j^{(n)} \right\} \right)$ using (33)
40.	repeat *Step 8* until $\Omega_{j^*} \cdot p_{j^*} \left(\tilde{s}_{ij^*} \left(Y_{j^*}^{(n+2)} \right) \right) \le SAR^{\text{limit}}$, $\forall j^*$ (*stopping criterion*)
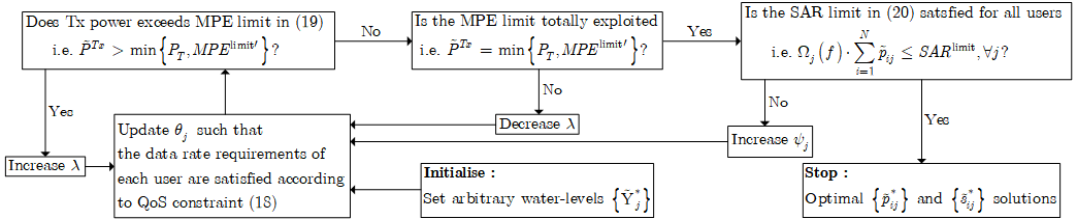
FIGURE 10 Block diagram of the proposed implementation algorithm.

water-levels $\left\{ \tilde{Y}_j^* \right\}$ in (33) to assign the initial values for the multipliers λ, ψ_j, and θ_j. That way, *Phase 1* obtains the initial water-levels and subcarrier allocations, i.e., $Y_j^{(0)}$, $\forall j$ and $\tilde{s}_{ij}\left(Y_j^{(0)}\right)$, $\forall i,j$, using the proposed power and subcarrier allocation formulas in (27) and (32), respectively. *Phase 2* proceeds using the bisection method to update $\lambda \to \lambda^{(n)}$. Since λ is inversely proportional to $Y_j^{(0)}$ (see e.g. (33)) we set lower and upper bounds for λ. If the radiated power at the BS exceeds the MPE limit, i.e., $P^{Tx}\left(Y_j^{(0)}\right) > MPE^{\text{limit}'}$, then P^{Tx} decreases and λ is inquired within a large region $(\lambda_{LB}^{(0)} = \delta, \lambda_{UB}^{(0)} = \Delta)$. On the other hand, if $P^{Tx}\left(Y_j^{(0)}\right) < MPE^{\text{limit}'}$, then P^{Tx} increases and λ is determined within a small region $(\lambda_{LB}^{(0)} = \lambda_{UB}^{(0)} = \delta)$. *Phase 2* is repeated until the available power at the BS is totally exploited i.e., $\lambda^{(0)} \to \lambda^{(n)}$ and $P^{Tx}\left(\tilde{s}_{ij}\left(Y_j^{(n)}\left(\lambda^{(n)}, \left\{\psi_j^{(0)}\right\}, \left\{\theta_j^{(0)}\right\}\right)\right)\right) = MPE^{\text{limit}'}$. Remark that the convergence of the outer loop in *Phase 1* and *Phase 2* is guaranteed because the radiated power P^{Tx} decreases monotonically with λ given that the target data rates and SAR for all users are satisfied.

Then, the algorithm initialises two inner loops to satisfy the QoS and MPE constraints of the individual users (i.e. (18) and (19), respectively). The first inner loop in *Phase 3* defines a set of potentially optimal users $\{j^*\}$ through the allocation strategy in *Theorem 1*. Given $\lambda^{(n)}$ and $\left\{\psi_j^{(0)}\right\}$ the algorithm uses bisection to update $\left\{\theta_{j^*}^{(0)}\right\} \to \left\{\theta_{j^*}^{(n)}\right\}$ until the data rate of each user j^* is equal to its minimum QoS requirement, i.e., $r_{j^*}\left(\tilde{s}_{ij^*}\left(Y_j^{(n+1)}\right)\right) = r_{j^*}^{\min}$. At each update of $\theta_j \to \theta_{j^*}^{(n)}$, the subcarrier allocation indexes are redefined as $\tilde{s}_{ij}\left(Y_j^{(0)}\right) \to \tilde{s}_{ij}\left(Y_{j^*}^{(n+1)}\left(\left(\lambda^{(n)}, \left\{\psi_j^{(0)}\right\}, \left\{\theta_{j^*}^{(n)}\right\}\right)\right)\right)$ and the process is repeated until both the QoS and the MPE constraints are satisfied. Remark that the convergence of *Phase 3* is guaranteed because $Y_j^{(n)}$ and H_{ij} increase monotonically with respect to θ_j meaning that for a user j^* more $\tilde{s}_{ij^*}$ become one and more data rate is allocated.

Furthermore, *Phase 4* is to manage the SAR level at each individual system user. If the SAR levels of all users are less or equal to the SAR^{limit}, which is set by constraint (20), the algorithm terminates and announces the joint optimal allocation strategy based on the obtained multipliers $\lambda^{(n)}$, $\left\{\theta_{j^*}^{(n)}\right\}$ and $\left\{\psi_{j^*}^{(0)}\right\}$. Otherwise, if some users have SAR levels above the considered thresholds, the algorithm updates the multipliers $\left\{\psi_{j^*}^{(0)}\right\} \to \left\{\psi_{j^*}^{(n)}\right\}$ and repeats the *Phases 2-4* until all of the constraints in (18), (19) and (20) are satisfied (stopping criterion). Remark that the convergence of *Phase 4* is ensured because channel gain matrix H_{ij^*} and SAR vector SAR_{j^*} decrease monotonically with respect to $\psi_{j^*}^{(0)}$ meaning that some $\tilde{s}_{ij^*}$s become zero and the corresponding SAR levels decrease, while the data rates of some users may decrease as some $\tilde{s}_{ij^*}$ change from one (allocated) to zero (not allocated). However, as all the Y_j's are monotonous with respect to multipliers λ, θ_j and ψ_j, the optimal water-level Y_j^*s can be approached iteratively [22].

references

[1] Public Health England, "WHO International EMF project: IAC meeting 06-07," Jun 2013

[2] M. Wyde, M. Cesta, C. Blystone, S. Elmore, P. Foster, M. Hooth, G. Kissling, D. Malarkey, R. Sills, M. Stout, N. Walker, K. Witt, M. Wolfe, J. Bucher, "Report of Partial findings from the National Toxicology Program Carcinogenesis Stud-

ies of Cell Phone Radiofrequency Radiation in Hsd: Sprague Dawley SD rats (Whole Body Exposure)", bioRxiv 055699, doi:https://doi.org/10.1101/055699, May 2016

[3] A. A. Salles, G. Bulla and C. E. Rodriguez, "Electromagnetic absorption in the head of adults and children due to mobile phone operation close to the head," *J. Electromagnetic Biological Medicine*, vol. 4, no. 25, pp. 349-360, 2006

[4] S. Cucurachi, W. L. M. Tamis, M. G. Vijver, W. J. G. M. Peijnenburg, J. F. B. Bolte, G. R. de Snoo, "A Review of the Ecological Effects of Radiofrequency Electromagnetic Fields (RF-EMF)," *Elsevier J. Environment International*, vol. 51, pp. 116-140, Jan 2013

[5] K. R. Foster and M. H. Repacholi, "Environmental Impacts of Electromagnetic Fields from Major Electrical Technologies," *International J. of Innovative Research in Science, Engineering and Technology*, vol. 5, no. 1, pp. 627-634, Jan 2016

[6] World Health Organization, "Electromagnetic Fields and Public Health: Mobile Phones", Technical Report, Fact sh. No 193, Aug 2014

[7] UK National Radiological Protection Board, "Restrictions on Human Exposure to Static and Time Varying Electromagnetic Rields and Radiation", Technical Report, vol. 4, no. 5, 1993

[8] US Federal Communications Commission, "Evaluating compliance with FCC guidelines for human exposure to radiofrequency electromagnetic fields", Technical Report, OET Bulletin 65, Supplement C, edition 01-01, 2001

[9] E. Yablonovitch, "Inhibited spontaneous emission in solid state physics and electronics," *Review Letters in Physics*, vol. 58, pp. 2059 - 2062, 1987

[10] J. Wang and O. Fujiwara, "Reduction of electromagnetic absorption in the human head for portable telephones by a ferrite sheet attachment," *IEEE Trans. Commun.*, vol. 80, no. 12, pp. 1810-1815, 1997

[11] A. Hirata, T. Adachi and T. Shiozawa, "Folded-loop antenna with a reflector for mobile handsets at 2.0 GHz," *Microwave Opt. Technol. Lett.*, vol. 40, no. 4, p. 272–275, 2004

[12] K. H. Chan, K. M. Chow, L. C. Fung and S. W. Leung, "Effects of using conductive materials for SAR reduction in mobile phones," *Microwave Opt. Technol. Lett*, vol. 44, no. 2, pp. 140-144, 2005

[13] J. B. Pendry, A. J. Holen, D. J. Robbins and W. J. Stewart, "Magnetism from conductors and enhanced nonlinear phenomena," *IEEE Trans. Microwave Theory Tech.*, vol. 47, no. 11, p. 2075–2084, 1999

[14] B. M. Hochwald and D. J. Love, "Minimizing exposure to electromagnetic radiation in portable devices," *Information Theory and Applications Workshop (ITA)*, pp. 255-261, 2012

[15] H. Dai, Y. Liu, G. Chen, X. Wu, T. He, A. Liu and Y. Zhao, "SCAPE: Safe Charging With Adjustable Power," *IEEE/ACM Trans. Netw.*, vol. 26, no. 1, pp. 520-533, Feb 2018

[16] T. D. Ponnimbaduge Perera, D. N. K. Jayakody, S. K. Sharma, S. Chatzinotas and J. Li, "Simultaneous Wireless Information and Power Transfer (SWIPT): Recent Advances and Future Challenges," *IEEE Communications Surveys & Tutorials*, vol. 20, no. 1, pp. 264-302, Jan 2018

[17] D. K. Nguyen, D. N. K. Jayakody, S. Chatzinotas, J. S. Thompson and J. Li, "Wireless Energy Harvesting Assisted Two-Way Cognitive Relay Networks: Protocol Design and Performance Analysis," *IEEE Access*, vol. 5, pp. 21447-21460, 2017

[18] C. Yang, J. Li, et. al. "Interference-Aware Energy Efficiency Maximization in 5G Ultra-Dense Networks", *IEEE Trans. Commun.*, vol. 65, no. 2, pp. 728 – 739, Feb 2017

[19] C. Zarakovitis, Q. Ni, J. Spiliotis. "Energy-Efficient Green Wireless Communication Systems With Imperfect CSI and Data Outage", *IEEE J. Sel Areas Commun.*, Vol. 34, Issue 12, pp. 3108 – 3126, Dec 2016

[20] C. Zarakovitis, Q. Ni, D. E. Skordoulis and M. G. Hadjinicolaou, "Power-Efficient Cross-Layer Design for OFDMA Systems with Heterogeneous QoS, Imperfect CSI and Outage Considerations", *IEEE Trans. Veh. Technol.*, vol. 61, no. 2, pp. 781-798, Feb 2012

[21] C. Zarakovitis, Q. Ni. "Maximizing Energy Efficiency in Multi-User Multi-Carrier Broadband Wireless Systems: Convex Relaxation and Global Optimization Techniques", *IEEE Trans. Veh. Technol.*, vol. 65, no. 7, pp. 5275 – 5286, July 2016

[22] M. Tao, Y. Liang, F. Zhang. "Resource allocation for delay differentiated traffic in multiuser OFDM systems", *IEEE Trans. Wireless Commun.*, Vol. 34, Issue 12, pp. 3108 – 3126, Dec 2016

[23] Q. Ni and C. C. Zarakovitis, "Nash Bargaining Game Theoretic Scheduling for Joint Channel and Power Allocation in Cognitive Radio Systems", *IEEE J. Sel. Areas Commun.*, vol. 30, no. 1, pp. 70-81, Jan 2012

[24] H. Pervaiz, et. al. "Energy and Spectrum Efficient Transmission Techniques under QoS Constraints toward Green Heterogeneous Networks", *IEEE Access*, vol. 3, pp. 1655 – 1671, Sept 2015

[25] S. Singh, M. Shahbazi, K. Pelechrinis, K. Sundaresan, S. Krishnamurthy and S. Addepalli. "Adaptive sub-carrier level power allocation in OFDMA networks", *IEEE Trans. Mobile Computing*, vol. 14, no. 1, pp. 28 – 41, Jan. 2015

[26] D. Hui, V. Lau and H. Wong, "Cross-layer design for OFDMA wireless systems with heterogeneous delay requirements", *IEEE Wireless Commun.*, vol. 6, no. 8, pp. 2872-2880, Aug 2007

[27] T. Zhang, Z. Zeng, C. Feng, J. Zheng and D. Ma, "Utility fair resource allocation based on game theory in OFDM systems", *IEEE ICCCN*, pp. 414-418, Aug 2007

[28] B. B. Kim and D. W. Kim, "Bandwidth enhancement for SSN suppression using a spiral-shaped power island and a modified EBG structure for a $\lambda/4$ open stub," *J. ETRI*, vol. 31, no. 2, p. 201–208, 2009

[29] S. I. Kwak, D. U. Sim, J. H. Kwon and H. D. Choi, "Experimental tests of SAR reduction on mobile using EBG structures," *Lett. Electron.*, vol. 44, no. 9, 2008

[30] S. Boyd and L. Vandenberghe, "Convex Optimization," Cambridge University Press, 2004

[31] World Health Organization, "IARC classifies radiofrequency electromagnetic fields as possibly carcinogenic to humans," Press Release No. 208 International Agency for Research on Cancer, 2011

Charilaos C. Zarakovitis received the B.Sc degree from the Technical University of Crete, Greece, in 2003, the M.Sc and G.C.Eng degrees from the Dublin Institute of Technology, Ireland, in 2004 and 2005, and the M.Phil and Ph.D degrees from Brunel University, London, UK, in 2006 and 2012, respectively, all in electronic engineering. He is currently Researcher with the School of Computing and Communications, Lancaster University, UK and with the Media Networks Laboratory, Institute of Informatics and Telecommunications, National Centre for Scientific Research "Demokritos", Greece. His main research interests include next generation green wireless networking, software defined networks, cognitive IoT architecture, visual light communications, statistical signal processing, game theoretical radio resource scheduling and convex optimisation analysis.

Qiang Ni received the B.Sc, M.Sc, and Ph.D degrees from the Huazhong University of Science and Technology (HUST), China, all in engineering. He is currently a Professor and the Head of the Communication Systems Group with InfoLab21, School of Computing and Communications, Lancaster University, Lancaster, UK. He has published over 200 papers. His main research interests lie in the area of future generation communications and networking, including green communications and networking, cognitive radios, heterogeneous networks, 5G, energy harvesting, IoT, and vehicular networks. He was an IEEE 802.11 wireless standard working group voting member and a contributor to the IEEE wireless standards.

Michail-Alexandros Kourtis received the M.Sc Diploma in Computer Science, and the Master's Degree in Computer Science from Athens University of Economics and Business Greece, in 2011 and 2014, respectively. Currently, he is pursuing his PhD at the Department of Communications Engineering, University of the Basque Country (UPV/EHU), Bilbao, Spain. Since January 2010 he has been member of the Media Networks Laboratory at the National Center for Scientific Research "Demokritos" Greece and he has participated in various research projects such as IORL. His research interests include video processing, video quality assessment, image processing, network function virtualisation, software defined networks and quality of service.